Rotor-Fuselage Interaction: Analysis and Validation with Experiment

John Berry
Aeroflightdynamics Directorate, US Army ATCOM
Langley Research Center, Virginia

Nicolas Bettschart
ONERA – Office National D'Étude et de Recherches Aérospatiales
Châtillon, France

ABSTRACT

The problem of rotor-fuselage aerodynamic interaction has to be considered in industry applications from various aspects. First, in order to increase helicopter speed and reduce operational costs, rotorcraft tend to be more and more compact, with a main rotor closer to the fuselage surface. This creates significant perturbations both on the main rotor and on the fuselage, including steady and unsteady effects due to blade and wake passage and perturbed inflow at the rotor disk. Furthermore, the main rotor wake affects the tail boom, empennage and anti-torque system. This has important consequences for helicopter control and vibrations at low speeds and also on tail rotor acoustics (main rotor wake-tail rotor interactions). This paper describes the cooperative work on this problem from both the theoretical and experimental aspects. Using experimental 3D velocity field and fuselage surface pressure measurements, three codes that model the interactions of a helicopter rotor with a fuselage are compared. These comparisons demonstrate some of the strengths and weaknesses of current models for the combined rotor-fuselage analysis.

INTRODUCTION

The aerodynamic environment of rotorcraft configurations is complex due to the nature of the airflow of both the rotating blade and wake systems as well as relatively bluff fuselage shapes characteristic of rotorcraft. Until recently, analysis of the coupled effects of the rotor and the fuselage have been addressed through linear superposition and empirical corrections. Recently methods have been developed to model the non-linear aerodynamic interaction of rotor and wake with the fuselage.

Two principal effects of the rotor-fuselage interaction are important in the design (or redesign) of rotorcraft. The first effect is that of the fuselage on the rotor. The change in onset flow to the rotor due to the fuselage is important in loading and wake strength. These differences, in turn, change the system vibratory excitation and response, operating conditions and trim, and also the radiation of acoustic pressures from the rotor.

The second principal effect of the aerodynamic interaction of the rotor and the fuselage is that of the rotor on the fuselage. The effect of the rotor on the fuselage is to produce both a change in the steady aerodynamic load as well as an unsteady loading on the surfaces of the fuselage. It is well known (reference 1) that the wake of the main rotor vastly changes the loading of the tail rotor in certain flight conditions. Close rotor-canopy spacing required in military designs for transportability can produce very high unsteady pressures on canopy surfaces that lead to poor fatigue life of these components. Fuselage trim also changes due to wake effects on the empennage.

At the Aeroflightdynamics Directorate (AFDD, US Army ATCOM) two theoretical methods were used to simulate rotor-fuselage interactions. The Rotor-Wake-Fuselage (RWF) code is an in-house developed code

Presented at the American Helicopter Society 53rd Annual Forum, Virginia Beach, VA, April 29-May 1, 1997.

for exploring methods of computing the combined rotor-fuselage problem. RWF couples a time-stepping vortex lattice method for the rotor blade and wake system with a source panel fuselage model. The other US code is a recent version of the Continuum Dynamics, Inc. Computation of Rotor Airloads in Forward flighT/Aeroacoustic Analysis (RotorCRAFT) code. This code couples a doublet-panel representation of the fuselage with the Constant Vorticity Contour (CVC) wake model. At ONERA, the PEIRF (Programme d'Etude d'Interaction Rotor/Fuselage) code was also developed to simulate this problem. This quasi-steady approach couples a fuselage code to a rotor code which assumes a periodic in time solution. The fuselage is simulated by a low-order panel method (source and doublet distribution). A module was specifically developed to compute the unsteady pressure component on the fuselage surface, which is mainly due to the blades and wake. The rotor is modeled by a lifting-line with a full free-wake analysis, using 2D airfoil tables to compute the compressible loads occurring on the blades. Coupling between these two simulations is performed until a periodic solution is achieved.

Experimental data from powered helicopter models were shared during this cooperation for comparing the analytical methods. Comparison with field velocity data is a means of assessing the accuracy of the free-wake methods embedded in these codes. A realistic 1/7.7 scaled Dauphin powered model was tested in the ONERA S2Ch wind tunnel (figure 1). From this model steady and unsteady pressure data on the fuselage were acquired. Also, 3D laser velocimeter (LV) data were acquired in two vertical planes. The first plane was taken at a downstream location through the hub and the second plane was taken at 0.42 radius downstream from the hub. These experimental data provide calibration points for the analytical models. Comparisons of code results to determine relative effects of rotor-on-fuselage interaction are shown in the Results section. Comparison of codes with experimental data allows the assessment of the accuracy of the codes in modeling the physics of the interactional effects. The comparison with experimental data also helps in establishing the relative importance of un-modeled effects such as regions of flow separation from the fuselage. A code-to-code comparison has also been made of the predicted geometry of the tip vortex. Comparisons of the surface pressures, both steady and unsteady, show the local impact of the effect of the rotor wake on the fuselage.

NOTATION

The coordinates used for this study are defined relative the wind tunnel axis system for the velocity field measurements and with a body-local coordinate system to identify pressure measurements on the fuselage.

α	Angle of attack, deg.
α_S	Shaft angle of attack, deg.
β	Blade flapping angle, relative to the hub plane, deg.
φ	Velocity potential, m^2/s
μ	Advance ratio, $\frac{U}{\Omega R}$, 0.20 nominal
θ	Blade pitch angle at 3/4 radius, degrees
ρ	Density, 1.225 nominal, kg/m^3
σ	Rotor area solidity, $\frac{bc}{\pi R}$, 0.0849
Ω	Rotational speed, 133 radians/s nominal
ψ	Rotor azimuth, relative to downstream aligned with the fuselage, degrees
b	Number of blades, 4
c	Blade chord, 0.05 m
C_P	Pressure coefficient, $\frac{P - P_\infty}{q_\infty}$
P	Pressure, Pa
P_∞	Static pressure, Pa
q_∞	Dynamic pressure, $\frac{1}{2}\rho U^2$, 245 Pa nominal, Pa
R	Radius of the blade, 0.75 m
u, v, w	Components of local velocity, downstream , right, and up positive, m/s

U	Onset velocity, 20 m/s nominal
V	Local velocity magnitude, m/s
x, y, z	Location components, downstream , right, and up positive, m
PSID	Pressure rating of transducer in lbf/in^2

ANALYSIS

The three analyses used in this study are based on Green's theorem that allows the transformation of 3D field distributions to 2D singularity distributions on the boundaries of the field. These singularities are normally seen as source, doublet, or vortex singularities. This is the underlying principle in panel and lattice methods. Two US codes, RWF and RotorCRAFT/AA, will be described. A French code, PEIRF, is also used in this study and is described here.

RWF Code

The RWF code was developed during graduate studies at the Georgia Institute of Technology supported by the US Army (reference 2 and 3). This singularity method coupled a source panel method (reference 4 and 5) and a vortex lattice method wake (reference 6). The vortex lattice that represents the rotor blade and wake was improved from the previous methods to include the effects of cyclic pitch, multiple blades, and a far-wake downwash model. The coupling of the paneled fuselage with the vortex lattice wake was done by using an impulsively started wake with no presumed geometry. The wake was developed with the full interaction of the fuselage source panels as the solution was incremented in time. Although not a production code, RWF has been used as a test bed to study improvements for interactional singularity methods.

For this study, azimuthal step sizes of both 4 and 8 degrees were computed. Although no significant change in the character of the predicted velocities was seen, the 4 degree solution is used for comparison. A distribution of 3 chordwise panels and 12 spanwise panels was used for the rotor to compute the bound circulation strengths. The rotor tip-path plane was defined based on measured flapping angles and shaft angle. Cyclic pitch was set from the measured control angles (shaft axis) and transformed to the tip-path plane. The code set the minimum core effective size to be 30 percent of the panel diagonal dimension for both the bound and free lattice cells. This number was used based on unpublished studies on the effects of this radius on velocities computed on planes adjacent to the lattice. The code was run for sufficient iterations to allow the rotor disk to pass the starting vortex. This criteria can be expressed as:

$$\psi = \frac{180x}{\mu\pi R}$$

where the forward velocity is related to the azimuthal increment needed to move the disk forward x in distance. In this study a distance of $2R$ gives a minimum of 573 degrees to meet this criteria.

RotorCRAFT Code

The RotorCRAFT/AA (Mod 1.0) code is a computer program that determines the overall performance, aerodynamic loading and aeroacoustic pressure signature of a rotor in steady forward flight given the rotor geometry and its flight condition (reference 7). The code also supplies other information including the circulation distribution on the rotor blades, the wake structure downstream of the rotor blades (as modeled by a full-span, Constant Vorticity Contour (CVC) free wake of Basic Curved Vortex Elements, see reference 8), and the load distribution across the blade span at each azimuth location (reference 9). The code can also perform a structural analysis of the blade to determine its mode shapes and natural frequencies and can be used to determine the far field sound pressure level and spectrum at user-specified locations.

In RotorCRAFT/AA the blade is modeled as a vortex lattice with compressibility correction using airfoil tables. The wake is modeled using a unique method based on curves of constant vorticity shed by the changes in bound circulation on the rotor blades. These curves are distributed in space and can form closed loops as the maxima and minima of the bound circulation shed by the blades change. The curves of vorticity are convected as a free-wake using local and global induced velocities. The fuselage is modeled as a collection of vortex panels. Similar to a bound vortex lattice, the influence of the vortex panels is computed on all aspects of the flow. A unique feature of this analysis

code is the implementation of a Fast Vortex technique that reduces the size of the influence matrices (reference 10), allowing faster processing of complex geometries.

For this study, azimuthal step sizes were varied from 15 degrees (24 steps/revolution) to 7.5 degrees (48 steps/revolution). The blade is represented by 1 chordwise panel and 30 spanwise panels. The code assumes an undistorted form for the initial wake and relaxes this geometry during iterations as the rotor is turned through 2 revolutions. Nominal selections for wake core size, distribution of tip and sheet filaments, and other control variables were set as recommended in the code documentation.

PEIRF Code

The PEIRF code is based on an iterative coupling between two singularity methods, one modeling the fuselage, the other one the rotor and its wake.

The fuselage code is a low order panel method (constant source and doublet distribution), developed at ONERA (reference 11). The sources intensities are explicitly given by the slip condition on the fuselage surface and they define the right hand side of a linear system of which the unknowns are the doublet strength.

The rotor code is a lifting line method with a vortex wake model. Initially developed by Eurocopter France (reference 12) and known as METAR (Modele d'ETude de l'Aérodynamique du Rotor) with a prescribed rotor wake, this code has been improved by ONERA which developed and validated the MESIR code (Mise en Equilibre du Sillage Rotor) with a full free wake approach (reference 13). In these codes, the blades are replaced by 25% chord lifting lines which take the actual geometry of the blade such as spanwise variation of chord, twist, sweep, anhedral, etc. into account. The rotor wake is modeled by lattices of spanwise and tangential vortices of constant strength; therefore, it is equivalent to a constant doublet distribution. The rotor aerodynamic solution is carried out by an iterative process initialized by a mean Meijer-Drees induced velocity; the lift is obtained through 2-D airfoil tables with the computed local Mach number and incidence and the circulation is calculated from the Joukowski law. The velocities induced by the new rotor wake strength can be computed by means of the Biot-Savart law. This iterative process is stopped when the variation of the induced velocities is less than a defined value (typically 0.001 m/s) from one iteration to another. The free wake computation implemented in the MESIR code is also based on a quasi-steady azimuthal marching process: the vortices forming the rotor wake are moved from one azimuthal position to the next one by taking into account the induced velocities from the rotor wake, the blades and the freestream. Because the rotor wake geometry changes from one revolution to another, the influence coefficients matrix should be reevaluated. In order to accelerate the process, the influence coefficients matrix is computed again only every three revolutions but the induced velocities and the singularity strengths carried by the rotor wake are computed, as described above, at each azimuth. In most applications, nine rotor revolutions are sufficient to converge the process based on the mean displacement of the wake from one iteration to another. The blade angles (flapping and pitch) are specified as input to the code.

The PEIRF code couples the two codes described above by an azimuthal marching technique (reference 14). Two overlapped loops are started on an initial configuration which could be a fuselage and a prescribed rotor wake (METAR type), a free rotor wake (MESIR type), or even a partially converged result of the PEIRF code. The internal loop distorts the rotor wake geometry considering the effects of the rotor, its wake, and the fuselage. The velocities induced by the blades and the rotor wake are computed using the MESIR module. The velocities induced by the source and doublet distributions on the fuselage are evaluated using the Hess and Smith formulation. Then the velocity and the new singularity distribution on the fuselage are evaluated with this new rotor wake geometry and the inner loop is repeated for each azimuth. The outer loop computes the circulation distribution on the lifting lines due to the new wake geometry using the iterative METAR/MESIR procedure and the influence coefficient matrix is computed again. An acceleration technique based on the far field/near field approach has been developed and has reduced the computational time by one third up to as much as one half (reference 14).

Finally, because the PEIRF code is

based on a quasi-steady hypothesis, a specific algorithm has been developed in order to compute the fuselage unsteady pressure. It is based on the development of the unsteady term in the Bernoulli equation. Details can be found in references 14 and 15. Unsteady fuselage pressures are computed using the unsteady Bernoulli equation:

$$C_P = 1 - \left(\frac{V}{U}\right)^2 - \frac{2}{U^2}\frac{\partial \varphi}{\partial t}.$$

The first two terms are referred to as the "quasi-steady" pressure. The last term is the "unsteady" term of the equation. The velocity potential unsteady contribution on the surface pressures comes from changes in potential from all components of the flow. Unsteady potential components include that from the bound circulation on the blade as it moves relative to the fuselage surface, that from the motion of the wake vorticity as it is convected relative to the fuselage, and terms from other singularities that change in strength with time. All of the codes include the "quasi-steady" contribution to unsteady fuselage pressures. The PEIRF code includes three unsteady potential contributions to the fuselage unsteady pressures: bound circulation, wake vorticity, and unsteady fuselage doublet strength.

Code Summary

A summary of the significant characteristics of the codes is given in the table below. These characteristics identify the model used to capture the significant interactional features of the aerodynamics of rotor-fuselage configurations.

EXPERIMENT

Model and Apparatus

Powered Dauphin (365N) Model:

The powered model consists of three components: a fiberglass fuselage shell, the internal rotor drive and control system and the model rotor system. The fiberglass shell is a 1/7.7 scale of the 365N model Dauphin helicopter. No simulation of secondary flows (engine inlet and exhaust or tail fan, for example) is attempted for this study. The internal drive and control system consists of a drive motor and electric control actuators for the blade pitch control via a swashplate. Two drive motors were used. During the velocity field survey and static pressure measurements, an electric motor was used, but to measure the unsteady pressures, a hydraulic motor was installed to minimize the electrical noise in the pressure transducer signal. The rotor system consists of a hub and four elastic blades. Flap, lag, and pitch are allowed about a single spherical bearing that retains the blade. The blades are rectangular planform with constant OA 209 airfoil section and linear twist of -8.8 degrees from the root cutout at 27.5% radius to the tip.

S2Ch Wind Tunnel:

The ONERA S2Ch wind tunnel is a 3 m diameter test section, open return wind tunnel. The test section is reduced by a flat floor section of 1.65 m width. The tunnel is capable of speeds up to 120 m/s with an average of 0.2% freestream turbulence levels. At the nominal speed used for this study, the tunnel is known to have a turbulence level of 0.27% . Good optical access in the test section allows implementation of laser velocity

Table of Code Characteristics

Characteristic	RWF	RotorCRAFT	PEIRF
Fuselage	Source Panel	Vortex Panel	Source & Doublet
Blade	Vortex Lattice	Vortex Lattice	Lifting Line
Compressibility	Prantl-Glauert	Airfoil Table	Airfoil Table
Wake	Vortex Lattice	Curved Vortex	Vortex Lattice
Tip Vortex	Fixed Core Radius	Fat Core Model	Fixed Core Radius

Significant Test Parameters

Parameter	Value	Units
Thrust Coefficient, C_T	0.0062	
Advance Ratio, μ	0.20	
Tip Speed, ΩR	100	m/s
Shaft Angle of Attack, α_S	-7.0	degrees
Fuselage Angle of Attack, α	-3.0	degrees
Collective Blade Pitch, θ_0	6.17	degrees
Longitudinal Blade Pitch, θ_{1S}	-2.98	degrees
Lateral Blade Pitch, θ_{1C}	-2.60	degrees
Blade Coning, β_0	2.63	degrees
Longitudinal Flapping, β_{1C}	5.45	degrees
Lateral Flapping, β_{1S}	-0.28	degrees

measurement systems. Figure 1 is a photograph of the powered Dauphin model in the S2Ch wind tunnel.

3D Laser Velocimeter:

For this study the ONERA has implemented a three component Laser Velocimeter (LV). This velocimeter uses light from 2 argon lasers (9 Watt), one for a violet beam (476.5 nm) at approximately 3 Watts, and another that is split into 2 principal colors (green at 514.5 nm and blue at 488 nm) with approximately 6 Watts in all lines. Once each color is split it is processed by sending one of the beams through a Bragg cell to apply a frequency shift. This frequency shift allows determination of the direction of travel for a particle passing through the fringes in the sample volume. The monochromatic beams are directed to one focused position in the test section at a focal length of approximately 2 m. The sample volume at this focused position is approximately spherical of diameter 0.4 mm. In this sample volume interference fringes are produced for each of the colors. Incense particles that seed the flow pass through the sample volume and scatter light with variation in amplitude corresponding to the light fringes. This scattered light is captured by two Cassegrain telescopes in backward scatter mode. The receive optics separate the three colors into pseudo-components and convert the optical signal into electrical signal with photo-detectors. Signals from the photo-detectors are processed by counters for frequency content. Velocities are derived from the frequency of the fringe modulation of the light signals. Pseudo components are converted to actual u, v, and w components using trigonometric relations of the physical characteristics of the optic system. The entire system is mounted on a three axis rigid table that is translated to move the measurement location in the tunnel up to 600 mm in each axis with 0.01mm accuracy.

Test Procedures

For this study only a single flight condition was evaluated. This flight condition is characteristic of moderate forward flight speed. At this condition the rotor wake is not expected to impact directly on the fuselage, but even so, its influence is expected to be significant. At this test condition, collective and cyclic blade pitch is set to a trim condition defined below.

The conventions during this study for the harmonic coefficients of blade pitch and blade flap are:

$$\theta = \theta_0 + \theta_{1C}\cos\psi - \theta_{1S}\sin\psi$$

$$\beta = \beta_0 - \beta_{1C}\cos\psi + \beta_{1S}\sin\psi .$$

Table of Balance Characteristics

Balance	S1S2		D91	
	Range	Accuracy	Range	Accuracy
X Force, N	1800	±40	250	±0.50
Y Force, N	4500	±4.5	200	±0.40
Z Force, N	2100	±3.0	2000	±4.00
L Moment, m N	250	±0.25	48	±0.10
M Moment, m N	80	±0.10	60	±0.12
N Moment, m N	140	±0.15	26	±0.05

The data for this study were acquired during several entries in the S2Ch wind tunnel. Changes in the model and instrumentation between entries will be described here.

Model measurements:

Model instrumentation consisted of a total balance that responds to both fuselage and rotor aerodynamic loading. Two force balances were used: during the first entry the S1S2 balance was used, during the second entry the D91 balance was used. Principal characteristics of these balances are given in the table of balance characteristics.

Field Velocity Measurement:

LV measurements were taken in two planes on the advancing side of the helicopter model. Optical access and significant effort in realigning the LV system would have been involved in measuring the retreating side. In the first plane, locations are distributed above and below the rotor. In the second plane, all measurements are below the rotor in locations to capture the wake velocity distributions.

Rotor azimuth was determined from a shaft encoder with 360 steps per revolution. Two measurement techniques were used during this study. For the first method, only the velocity field of one blade is captured by limiting the acquisition of signals to an azimuth range of $45 < \psi < 135$ degrees. At each measurement location, the measurement consisted of 100 particles for every increment of 2 degrees of azimuth, resulting in 45 increments of azimuth. In the second measurement technique, the azimuth window was open for the entire revolution, capturing the velocity field information for all four blades. In this case, 4 degree azimuth increments were used, resulting in 90 increments of azimuth.

Accuracy for the LV system used in this configuration is stated to have a relative error of 0.3% of the measured velocity. The precision of the measurement is on the order of 0.2 m/s.

Static Surface Pressure Measurement:

A distribution of 238 pressure taps were made on the surface of the model shell. The locations for these taps is shown in figure 2-1. Tubes from these taps were connected to a 6 head scanning valve with a Druck 1 PSID pressure transducer. During a pressure measurement, each port was sampled for 0.5 seconds after settling for 2 seconds. Pressure measurement errors are introduced by accuracy of the individual transducer, the reference pressure system, and also by the processing of the signal from the transducer. The stated precision of the static pressure measurements is 10 Pa.

Unsteady Pressure Measurement:

Another test entry in the S2Ch tunnel was made with another fuselage shell that included 44 dynamic pressure transducers directly on the surface of the fuselage shell. Locations for these transducers are shown in figure 2-2. The range of the transducers used was 2 PSID. During measurement of unsteady pressure, the signal from the transducer was sampled at 64 times per rotor revolution. Unsteady pressures can contain errors due to the accuracy and frequency

response of the individual transducers, the reference pressure, timing of the samples relative to the blade azimuth, as well as the dynamic characteristics of filtering and analog to digital conversion during the acquisition process. The stated precision of the unsteady pressures is 10 Pa.

RESULTS

Comparisons between experimentally obtained data and predicted results from rotor aerodynamic codes are shown here. In some instances where experimental data are not available, the comparison is made only between the predictive methods.

Field Velocities

Ten locations have been chosen for detailed comparison of the available methods. In the forward velocity measurement plane, four locations on each side of the model have been chosen. Two locations are 7% radius above the hub plane (at 75% and 107% radius) and two locations are 4% radius below the hub plane. On the retreating blade side of the model, these four locations are mirrored. In the plane located 42% radius behind the hub, one location on each side of the fuselage, relatively close to the fuselage, has been chosen.

The comparisons of azimuth dependent velocity are shown in figures 3-1 through 3-10. The first four figures include the experimental velocities. This set of velocities was taken with full azimuth of the rotor with a resolution of 4 degrees of azimuthal resolution. In the next four figures (3-5 through 3-8), there are no experimental data for comparison (retreating side of the model). Figures 3-9 and 3-10 are on the advancing side and retreating side of the tail in the 42% radius plane. Again, experimental data are only available on the advancing side.

The predictive methods are shown in all of the locations and represent the state-of-the-art in singularity methods for rotorcraft analysis. Unfortunately, the predictive methods did not use the same increments of azimuthal resolution. The RWF code was run with the highest resolution (4 degrees), while the PEIRF code was run with the lowest (15 degrees) of the three. Running the RWF code at such a high resolution prevented attainment of true periodicity. In the figures that follow, subsequent blade passages shown for the RWF code predictions are much closer to a representation of periodic solution.

In figures 3-1 and 3-5 the flow above and outboard the rotor disk is observed. Little variation in downstream component is seen with the mean value very close to the freestream value (20 m/s). Most of the variation is seen in the w, (vertical) component of velocity with a 4 per revolution variation of approximately 1 m/s peak-to-peak. None of the codes predict this magnitude of variation, or even the mean value of this component. Even the small magnitude of the cross-flow component of velocity is missed in sign by the methods. This location may be very sensitive to the location of the tip vortices from the previous blades where even a small change in relative position can significantly effect this measurement.

In figure 3-2 and 3-6, the velocity above the lifting portion of the rotor blade/disk is observed. In contrast to the observed velocities outboard of the tip, there is a strong periodic content in the u and w components of velocity, indicating the passage of a vortex or circulation oriented principally in the y direction. The impulsive acceleration in the u component indicates that the bound circulation on the blade passed under the measurement location. The “up-down” spike in the w component also confirms passage of bound circulation. The RWF and CDI codes capture, but under predict, the magnitude of the downstream velocity spike, indicating that the location of the blade to the measurement location may be closer than the geometry seems to indicate. The PEIRF code may not have enough azimuthal resolution to predict this impulsive behavior. For the lateral component of velocity, the experimental measurement indicates very little periodic content, while the PEIRF and RWF models predict significant variation. This may be due to the lattice model used for the “inboard sheet” of vorticity. The passage of lines of vorticity that represent the sheet vorticity can produce these periodic variations that are non-physical. The inboard sheet model of the CDI code seems to model this particular region to a much better degree. This localized effect of a vortex lattice sheet may also be an explanation for some of the velocity perturbation in vertical flow predicted by RWF here. On the retreating side of the disk, figure 3-6, the u

component of velocity sees a spike of the opposite polarity indicating the change in sign of the bound circulation passing the measurement point.

In figures 3-3, 3-4, 3-7, and 3-8 similar characteristics can be observed. A surprising correlation of all of the methods with the u component of velocity is seen in figure 3-4, while the other two components demonstrate either mean value or phase discrepancies.

In figures 3-9 and 3-10, there is little evidence that the measurement location experiences any close vortex passage. Each of the codes seem to miss the measured mean value of at least one component of velocity by approximately 1 m/s.

Velocity field prediction methods are still very sensitive to wake geometry accuracy. Although all of the methods use a free-wake model, the actual geometry of the wake will significantly affect the predicted velocity field in the neighborhood of the wake.

Wake Geometry

Due to the discrepancies noted in the velocity field predictions, a comparison of the wake geometry predictions is warranted. Unfortunately, the actual wake geometry and the RWF code wake data are not available. A comparison with the predicted tip vortex geometry predicted by CDI and PEIRF codes is of some value.

Predicted wake shapes of a tip filament from one blade with the rotor stopped at four azimuths are shown in figures 4-1 through 4-4. In these figures three views of the geometry are shown along with a plot of vertical deflection versus wake age.

Figure 4-1 shows the tip filament when the rotor is stopped at azimuth of 0. The three subsequent figures, 4-2, 4-3, and 4-4 progressively show the rotor tip filaments with the rotor at azimuths of 90, 180, and 270 degrees, respectively. In each figure there are four plots, counterclockwise from the top-left plot they are: top view (Y versus X), side view (Z versus X), back view (Z versus Y), and wake age (Z versus azimuth since released from the blade). In the two lower plots, the Z scale is multiplied by 2 to expand the vertical distortion.

One potentially significant observation is the starting location for the filaments. In the PEIRF model for the wake, the wake is trailed from the 1/4 chord of the blade tip. The RotorCRAFT code, however, begins the trailed filaments at the trailing edge of the blade at radial locations governed by the gradients of circulation on the blade. The dependence of the wake evolution is strongly dependent on the starting locations of these tip vortex filaments. Once these filaments are unbound from the blade, their local convection is dominated by local interactions with the tip vortices shed from previous blades.

The total age of the two methods are also different. This specific run of RotorCRAFT includes only two revolutions of converged wake, while PEIRF includes three revolutions. The difference in azimuthal step size can also be seen in the more abrupt changes in the CDI vertical displacement.

Vertical displacement of the wake due to the influence of the fuselage is also seen in these figures. This is seen in the rear (Y versus Z) view and wake age plot. In the wake age plot, a small effect of the fuselage is noticeable at age 180 degrees and more prominent vertical displacement occurs at age of 360, 540, and 720 degrees for figures 4-1 and 4-3. The similar effect in figures 4-2 and 4-4 is seen at 270, 450, and 630 degrees.

Also shown in figures 4-1 through 4-4 is a tip vortex geometry that is void of perturbation due to wake or fuselage. This trajectory is from the METAR model used to initiate the PEIRF code. The only vertical displacement is due to the component of freestream normal to the rotor disk and a uniform distribution of thrust induced velocity from the Meijer-Drees inflow model.

Without verification from experimental wake geometry, the accuracy in the geometric models must be assessed subjectively from information such as the velocity field or unsteady pressure data comparison.

Surface Pressures

Surface pressures for a powered model fuselage are characterized by two components, the steady part and the unsteady part. Several reasons can be given for presenting these parts separately. First, the measurement of these data were completed in several wind tunnel entries using different

pressure instrumentation. Second, the dynamic range of the unsteady part is significantly smaller than the mean component. Plotting scales may mask the unsteady component by the magnitude of the steady offset.

In figure 5-1 the experimental pressure coefficients along the dorsal line of the fuselage is compared with the prediction from the CDI and PEIRF programs. The experimental pressure values were taken from both the test using static pressure ports and the average of the data from the unsteady pressure test. Both codes used the same mesh of approximately 3000 panels for the fuselage. Over the nose the comparison between the codes and both experimental values are reasonable. At a station just ahead of the 500 mm location, the codes predict a significant difference in C_P. The CDI code predicts that the flow will stagnate at this body juncture while the PEIRF code does not predict any deceleration of the flow. There is a single data point with a C_P value of approximately 0.0 just behind the hub location where separation is expected but not included in the panel model used by the codes. The panel methods also predict a higher acceleration in the region of the hub. Without a model for the hub and its separation, this acceleration of the flow is expected to be different from the measured values.

In the region downstream of the hub there is some discrepancy between the steady pressure values shown in figure 5-1 and the average of the unsteady pressure data. In this region some flow separation is expected and may account for some of the measurement differences. The prediction of the codes is also in some disagreement with the data due to this separation that the codes are not accounting for. Over the tail boom there clearly is a discrepancy between the two codes in the region of strongest influence of the rotor wake. Although the CDI values for pressure are nominally closest to the experimental value, the effect of the hub region separation on this comparison has not been determined. In general, both codes do a reasonable job of predicting the steady component of pressure with the effects of a rotor at this speed.

Unsteady pressure comparisons are shown in figures 5-2 to 5-6. In each of these figures the perturbation pressure (mean removed) is compared as a function of rotor azimuth. Figure 5-2 shows the unsteady pressures at five locations at the section cut A-A (140 mm from the nose of the model). Both codes agree with each other in amplitude and phase of the unsteady pressures at the sides of this section cut. There is a 180 degree phase disagreement with the experimental values on the starboard side (retreating blade side) of this section. Additionally, both codes are in disagreement with the amplitude of the experimental pressures over the top of this section.

In figures 5-3 to 5-6 unsteady pressures are shown at selected locations from the section cuts at B-B (240 mm), D-D (735 mm), E-E (885 mm), and F-F (1035 mm). From all of these locations only 5 locations (19, 20, 33, 34, and 35) from two cuts (D-D and F-F) were shown to have acceptable correlation with the PEIRF code in both phase and amplitude. The locations at section F-F have the most direct physical relation between the section of the rotor blade with the highest loading and transducer location. Here the unsteady potential term, $\frac{\partial \varphi}{\partial t}$, due to close passage of the bound circulation (local lift) with very high relative velocity, is expected to dominate the unsteady pressure. This location is also downstream of the hub region, where the presence of the hub could diffuse any structure of the strong tip vortex from the leading half of the rotor disk. At other locations strong contributions are expected from both passage of the bound circulation on the blade and the convection of the strong tip vortex at lower speed (approximately freestream) but with closer spacing to the transducers. Accurately predicting the phase and amplitude of these two sources is still in question.

CONCLUSIONS

Comparisons have been made with three analytical methods and a unique set of experimental data. The Rotor-Wake-Fuselage (RWF) code is an AFDD in-house developed code for exploring methods of computing the combined rotor-fuselage problem. . The other US code is a recent version of the Continuum Dynamics, Inc. Computation of Rotor Airloads in Forward flighT/Aeroacoustic Analysis (RotorCRAFT)

code. At ONERA, the PEIRF (Programme d'Etude d'Interaction Rotor/Fuselage) code was also developed to simulate this problem. The effects of the rotor wake on the flowfield of a helicopter have been assessed using experimental data and the predictions of these codes. The significant observations are:

1. From the field velocity comparisons, locations where blade bound circulation and tip vortex come close give good indications to the relative location and strength of the vorticity. However, lattice models for the wake used by RWF and PEIRF codes produced unexpected periodic velocities when the filaments of the sheet are convected close to the measurement location.

2. The geometry of the tip vortex predicted by the codes has only been compared between codes. The wake evolution is strongly dependent on the starting locations of these tip vortex filaments. The larger azimuthal step size results in the more abrupt changes in vertical displacement. Comparison with experimental wake geometry data is needed to resolve additional differences between the code methods.

3. In general, the CDI and PEIRF codes do a reasonable job of predicting the steady component of pressure with the effects of a rotor at this speed. Without a model for the hub and its separation, the flow predicted by the codes is expected to be different from the measured values in the hub region.

4. Over the tail boom there is clearly a discrepancy in steady pressure values between the two codes in the region of strongest influence of the rotor wake. Although the CDI values for pressure are nominally closest to the experimental value, the effect of the hub region separation on this comparison has not been determined.

5. The PEIRF code matched experimental values of unsteady pressure very closely at only 5 of the points examined in this study while the CDI code did not show even this level of correlation. The locations on the tailboom top, where this correlation is best, have the most direct physical relation between the section of the rotor blade with the highest loading and transducer location. Here the unsteady potential term due to close passage of the lifting sections of the blade is expected to dominate the unsteady pressure. At other locations contributions to the measured unsteady pressure due to passage of the strong tip vortex and the bound circulation of the blade cannot be separated.

ACKNOWLEDGMENTS

The authors wish to acknowledge the significant contributions of the S2 Chalais-Meudon wind tunnel team and Eurocopter France for technical support of the experiments. This study was partially supported by the Service Technique des Programmes Aeronautiques (STPA) and Direction des Recherches, Etudes et Techniques (DRET). The study was also supported in part by the National Aeronautics and Space Administration, Langley Research Center.

REFERENCES

1. Prouty, R. W.: Helicopter Aerodynamics, PJS Publications, 1985.

2. Berry, J.: "A Method of Computing the Aerodynamic Interactions of a Rotor-Fuselage Configuration in Forward Flight", PhD Dissertation, Georgia Institute of Technology, May 1990.

3. Berry, J.: "A Multi-Element Vortex Lattice Method for Calculating the Geometry and Effects of a Helicopter Rotor in Forward Flight", 26th AIAA Applied Sciences Meeting, Reno, NV, 1988. (AIAA 88-86-0336)

4. Hess, J. L. and Smith, A. M. O.: "Calculations of Non-lifting Potential Flow About Arbitrary Three-Dimensional Bodies", Douglas Airdraft Company Report E. S. 40622, March 1962.

5. Hess, J., and Smith, A. M. O.: "Calculation of Potential Flow About Arbitrary Bodies", Vol. 8 of Progress in Aeronautical Sciences, Pergamon Press, Oxford and New York, 1966

6. Crispin, Y.: "Computing the Wake of a Rotor in Forward Flight", AIAA paper 82-8000, 1982.

7. Wachspress, D. A., Quackenbush, T. R., Boschitsch, A. H. and Lam, C-M. G.: "RotorCRAFT/AA (Mod 1.0) User's Manual", Continuum Dynamics, Inc.

Technical Note No. 95-23, February 1996.

8. Bliss, D. B., Teske, M. E., and Quackenbush, T. R.: "A New Methodology for Free Wake Analysis Using Curved Vortex Elements", NASA Contractor Report 3958, December 1987 (also Continuum Dynamics, Inc. Report No. 84-6, May 1984).

9. Quackenbush, T. R., Bliss, D. B., Wachpress, D. A., Boschitsch, A. H., and Chua, K. C.: "Computation of Rotor Aerodynamic Loading in Forward Flight using a Full-Span Free Wake Analysis", NASA Contractor Report 177611, October 1990 (also Continuum Dynamics, Inc. Report No. 90-05, Dec. 1990).

10. Chua, K. and Quackenbush, T. R.: "Fast Vortex Technology (FVT Mod 1), Theory Documentation, Software User's Manual, Programmers' Manual", Continuum Dynamics, Inc. Report No. 91-06P, December 1991.

11. Ryan, J., Falempin, G., Le TH.: "Rotor Plane Velocities Induced by a Helicopter Fuselage", Presented at the Second Helicopter Basic Research Conference, Army Research Office, College Park, MD, 1988.

12. Dehondt, A., Toulmay, F.: "Influence of Fuselage on Rotor Inflow Performance and Trim", Presented at the 15th European Rotorcraft Forum, Amsterdam, 1989.

13. Michea, B., Desopper, A., Costes, M.: "Aerodynamic Rotor Loads Prediction Method with Free Wake Analysis for Low Speed Descent Flights", Presented at the 18th European Rotorcraft Forum, Avignon, 1992.

14. Bettschart, N., Gasser, D.: "Analysis of Helicopter Rotor-Fuselage Interaction", Presented at the 20th European Rotorcraft Forum, 1994.

15. Gasser, D., Bettschart, N., Drouin, B.: "Theoretical and Experimental Studies on Unsteady Helicopter Interactional Aerodynamics", Presented at the American Helicopter Society, Vertical Lift Aircraft Design Conference, San Francisco, CA, 1995.

Figure 1: Dauphine Model in S2Ch Wind Tunnel

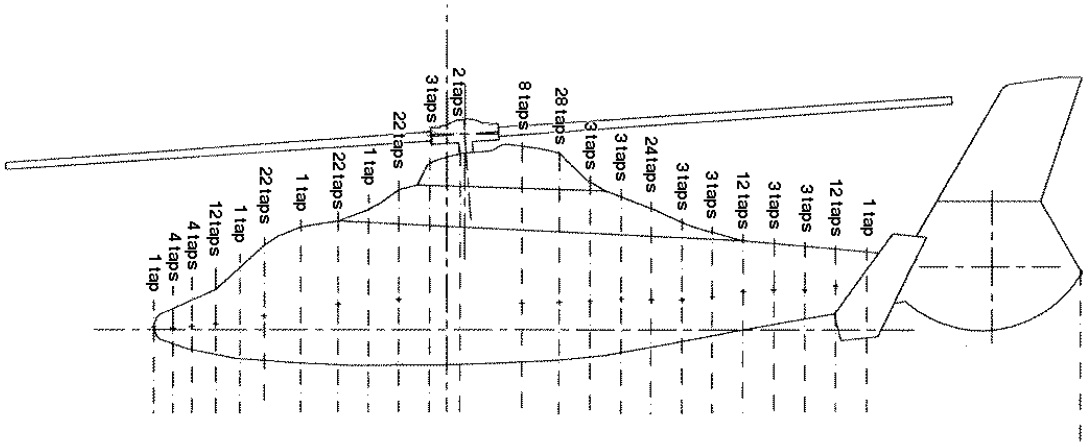

Figure 2-1: Locations of Pressure Ports

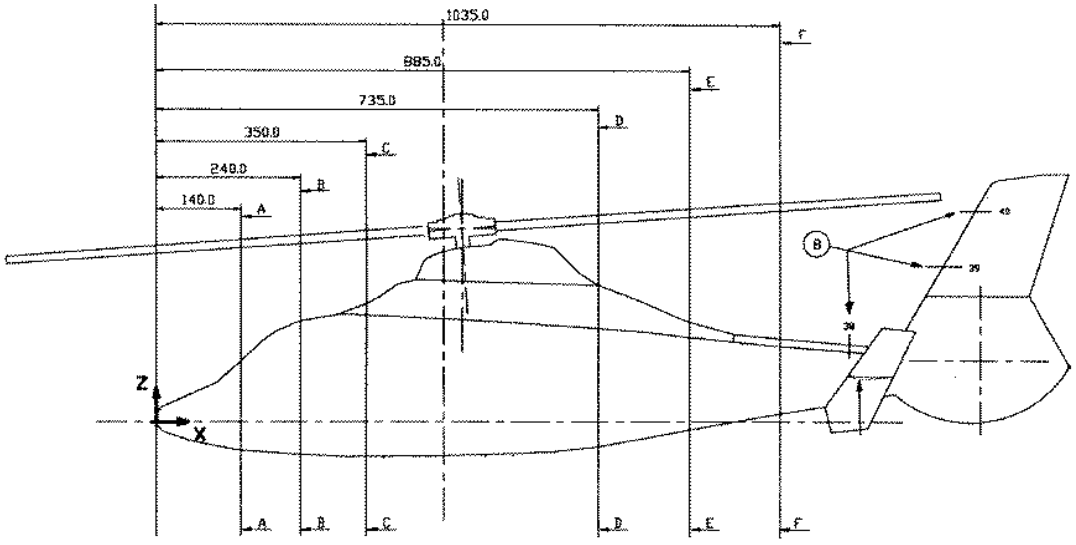

Figure 2-2: Locations of Unsteady Pressure Taps

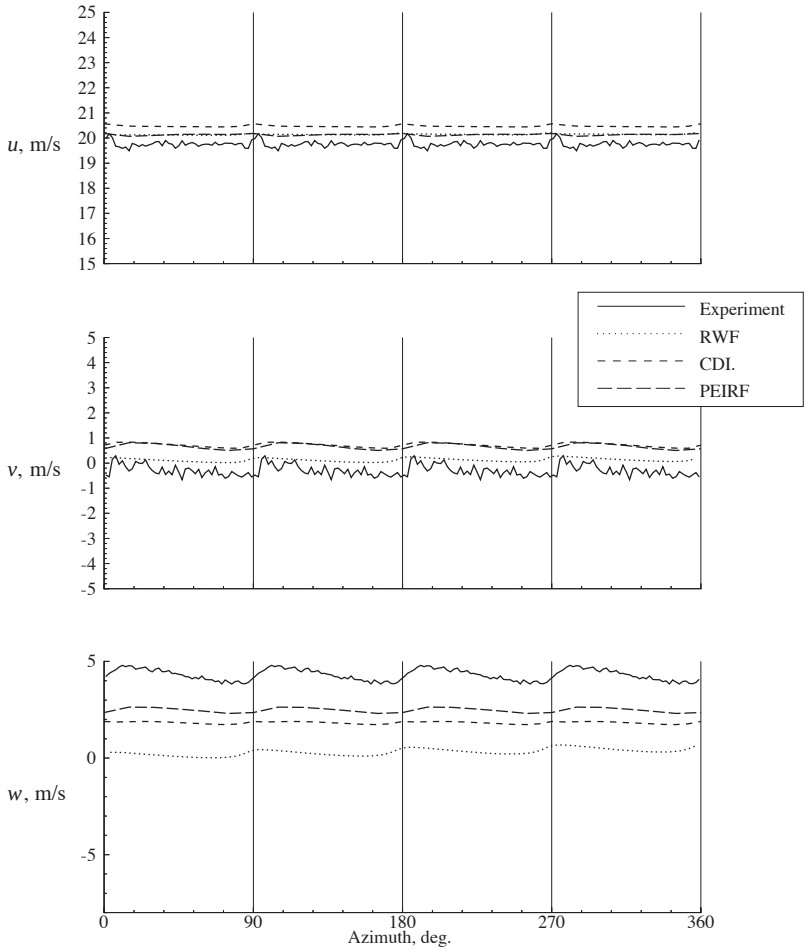

Figure 3-1: Velocity at x =0.0 R; y=-1.07 R; z=0.07 R

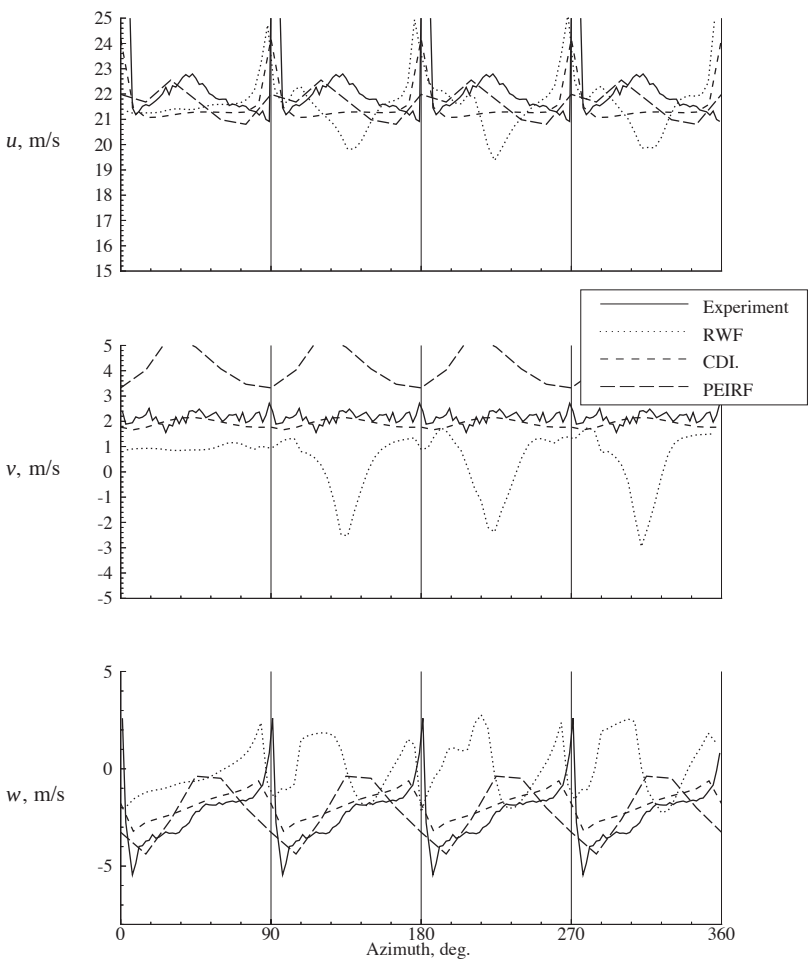

Figure 3-2: Velocity at x =0.0 R; y=-0.75 R; z=0.07 R

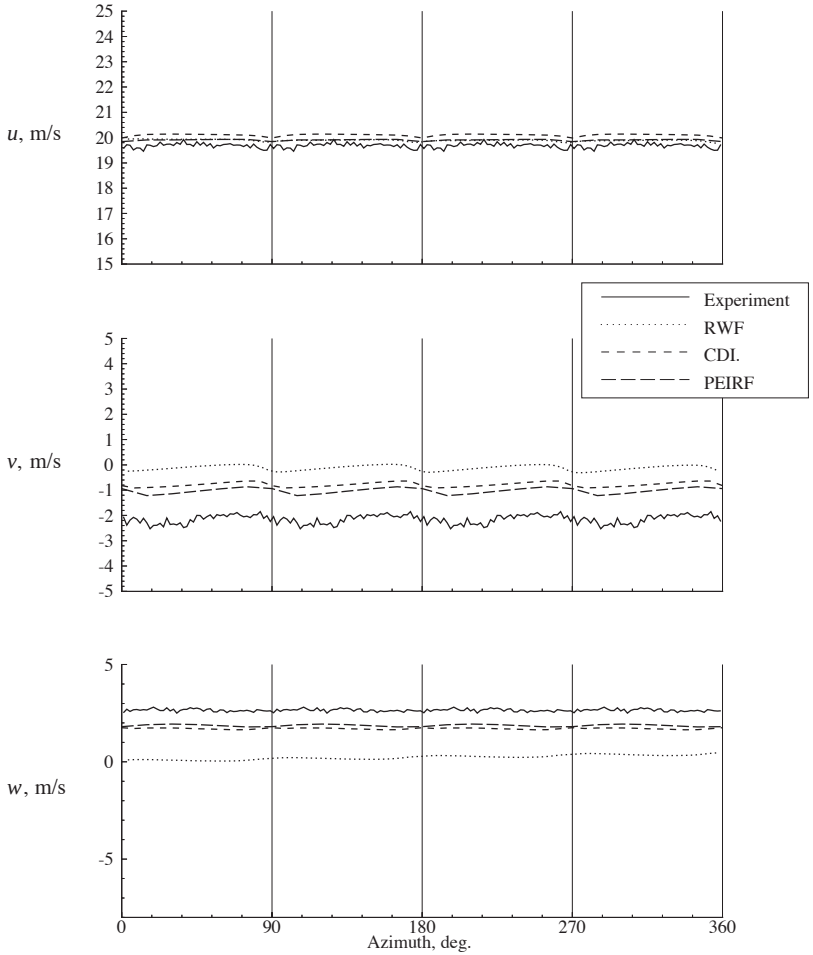

Figure 3-3: Velocity at x =0.0 R; y=-1.07 R; z=-0.04 R

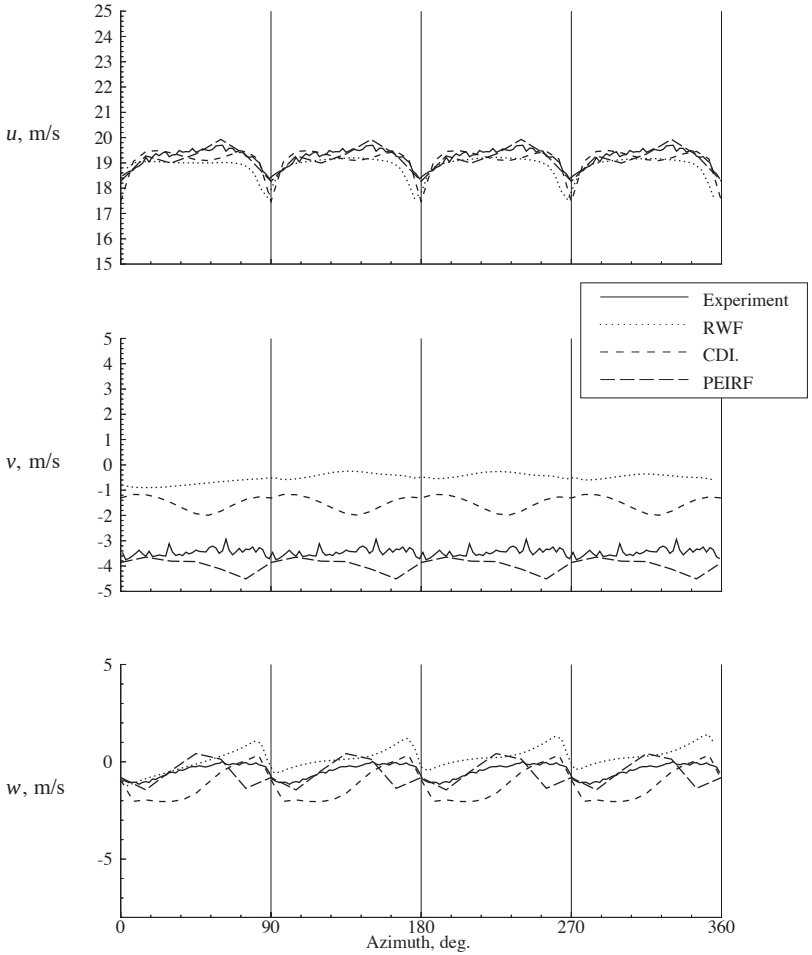

Figure 3-4: Velocity at x =0.0 R; y=-0.75 R; z=-0.04 R

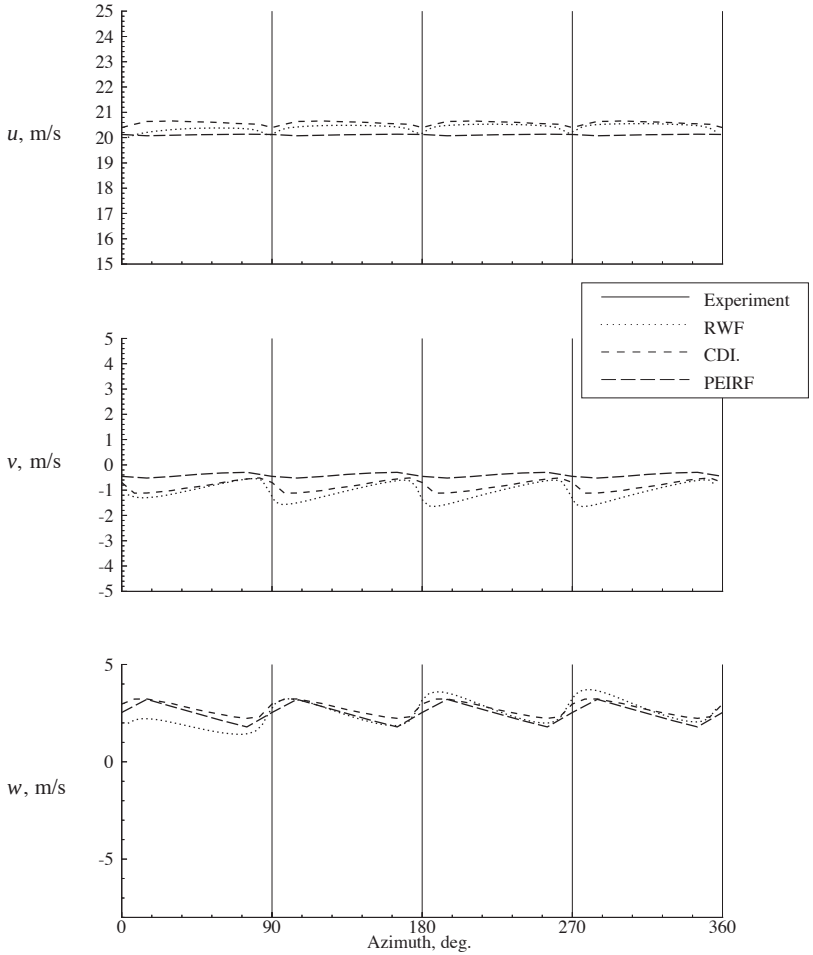

Figure 3-5: Velocity at x =0.0 R; y=1.07 R; z=0.07 R

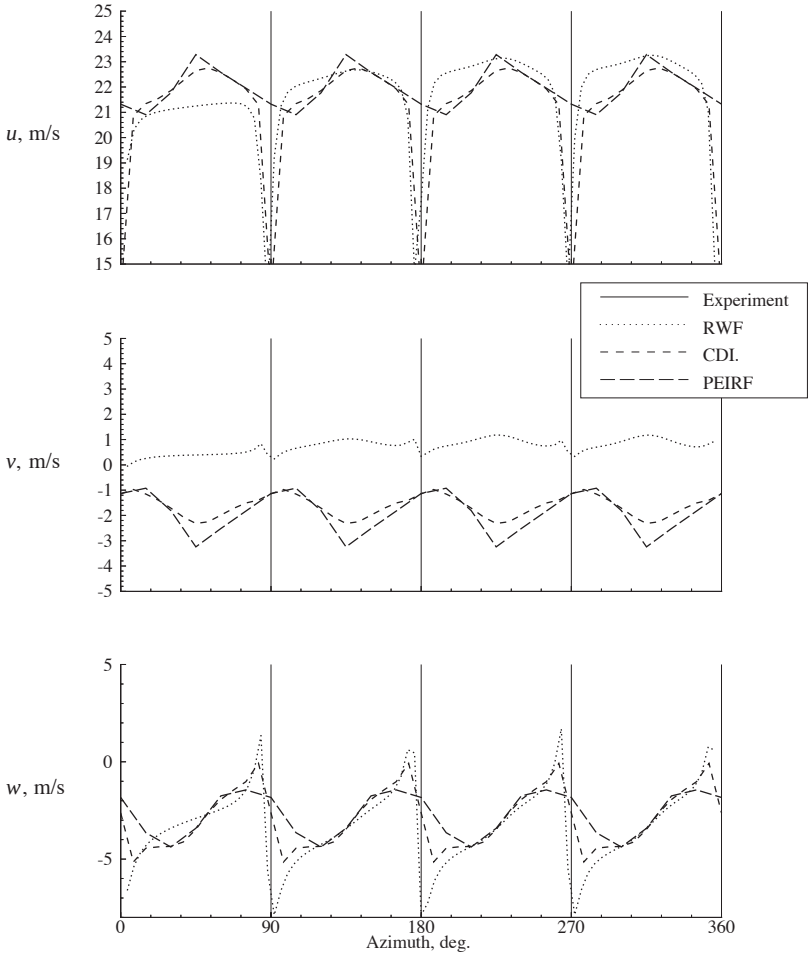

Figure 3-6: Velocity at x =0.0 R; y=0.75 R; z=0.07 R

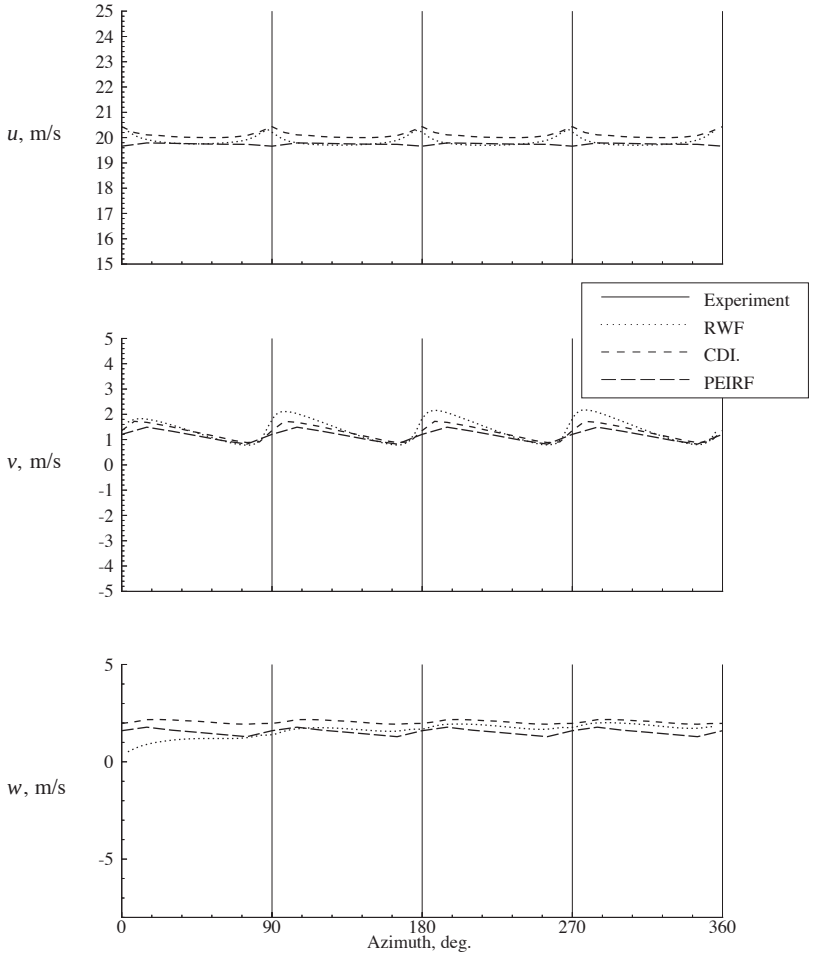

Figure 3-7: Velocity at x =0.0 R; y=1.07 R; z=-0.04 R

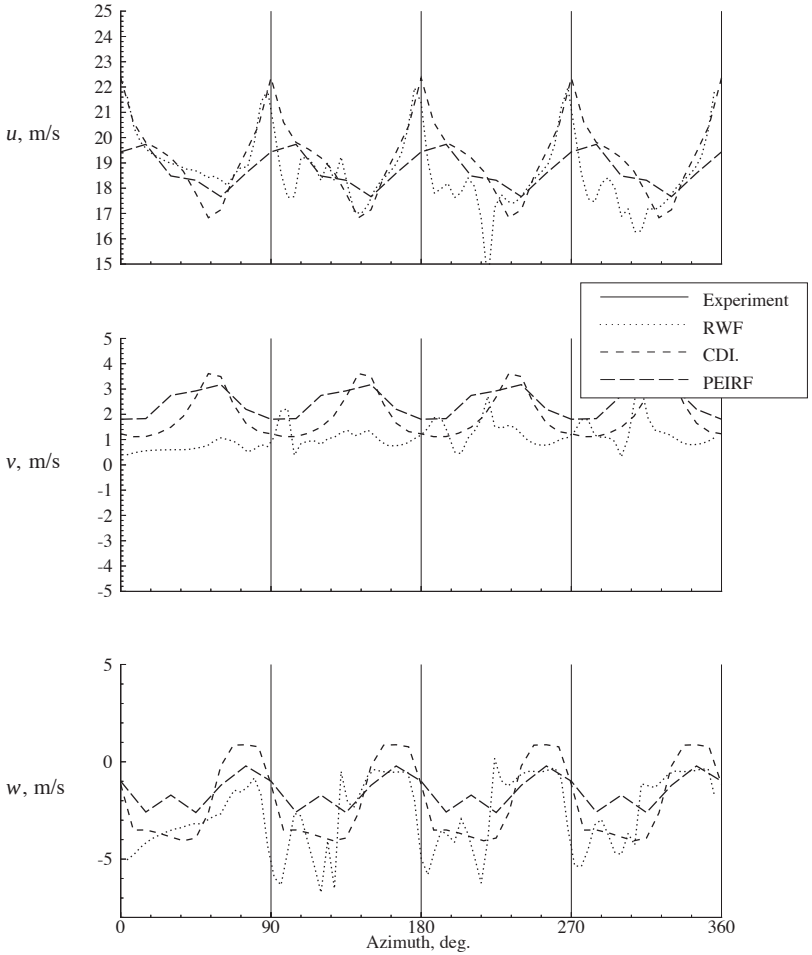

Figure 3-8: Velocity at x =0.0 R; y=0.75 R; z=-0.04 R

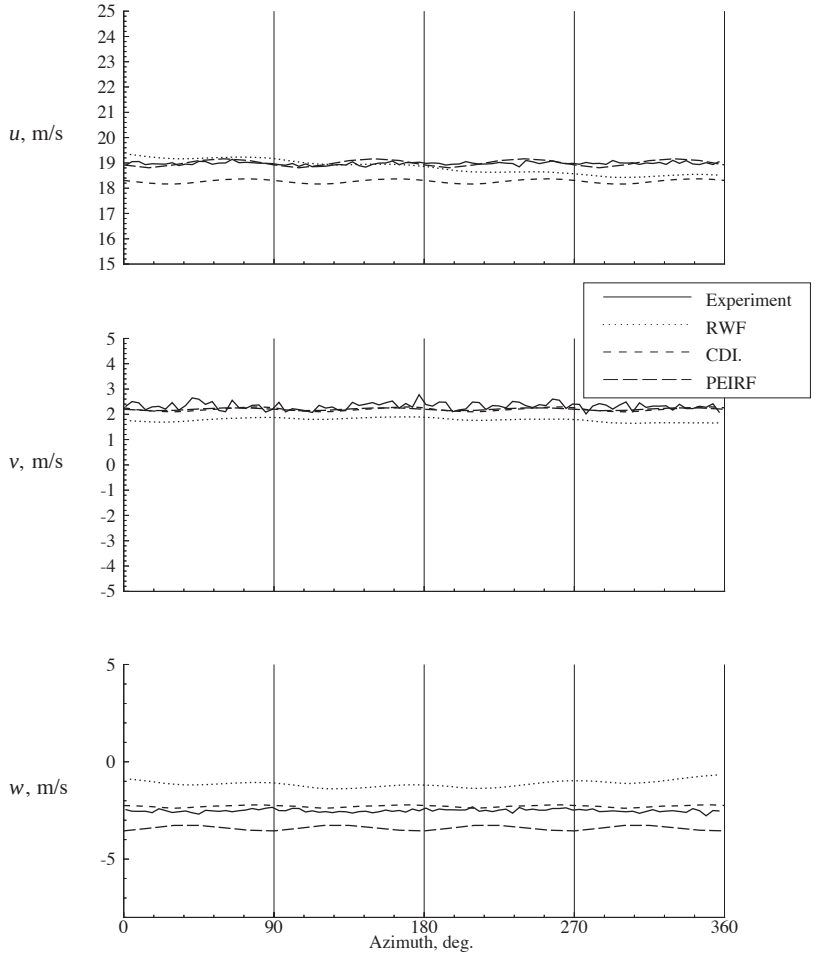

Figure 3-9: Velocity at x =0.42 R; y=-0.19 R; z=-0.35 R

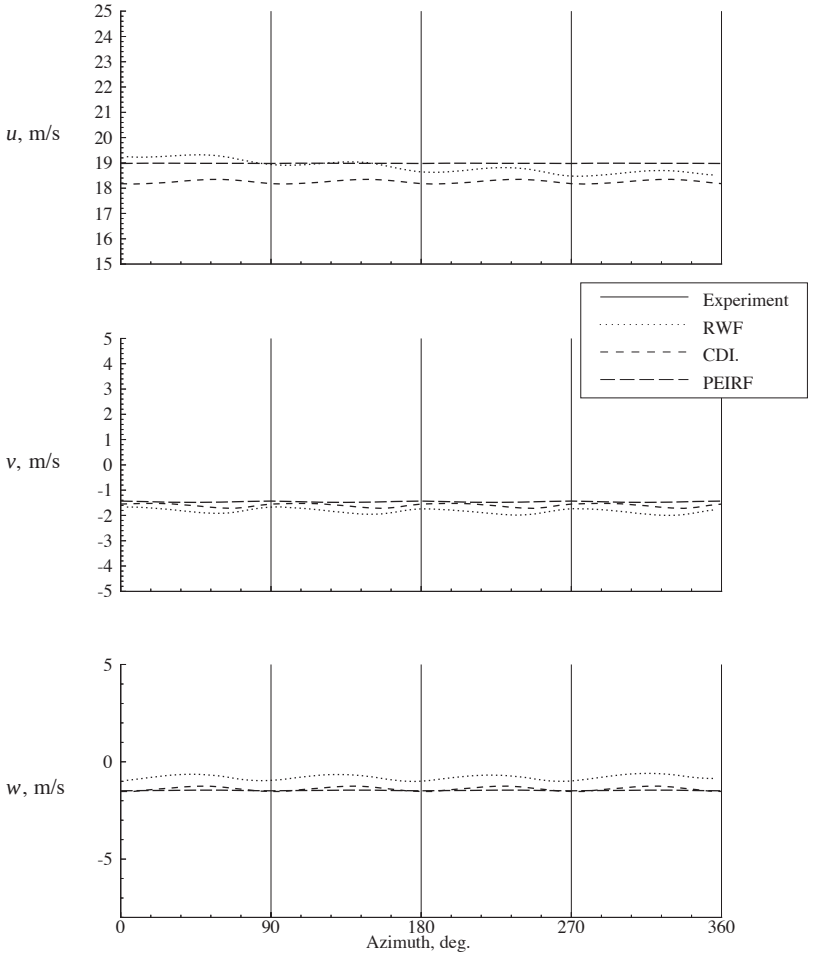

Figure 3-10: Velocity at x =0.42 R; y=0.19 R; z=-0.35 R

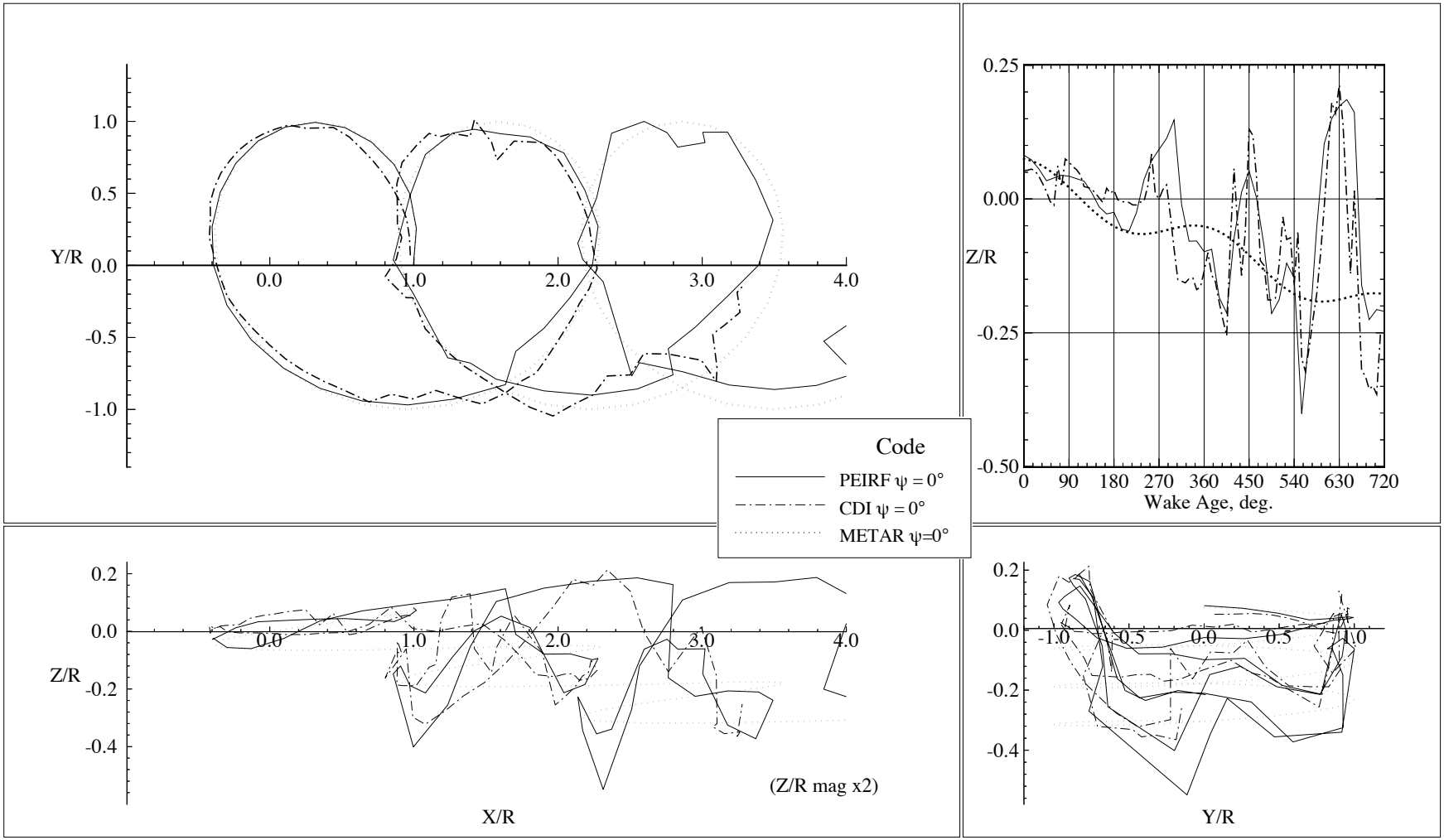

Figure 4-1: Wake geometry with rotor at ψ=0.0

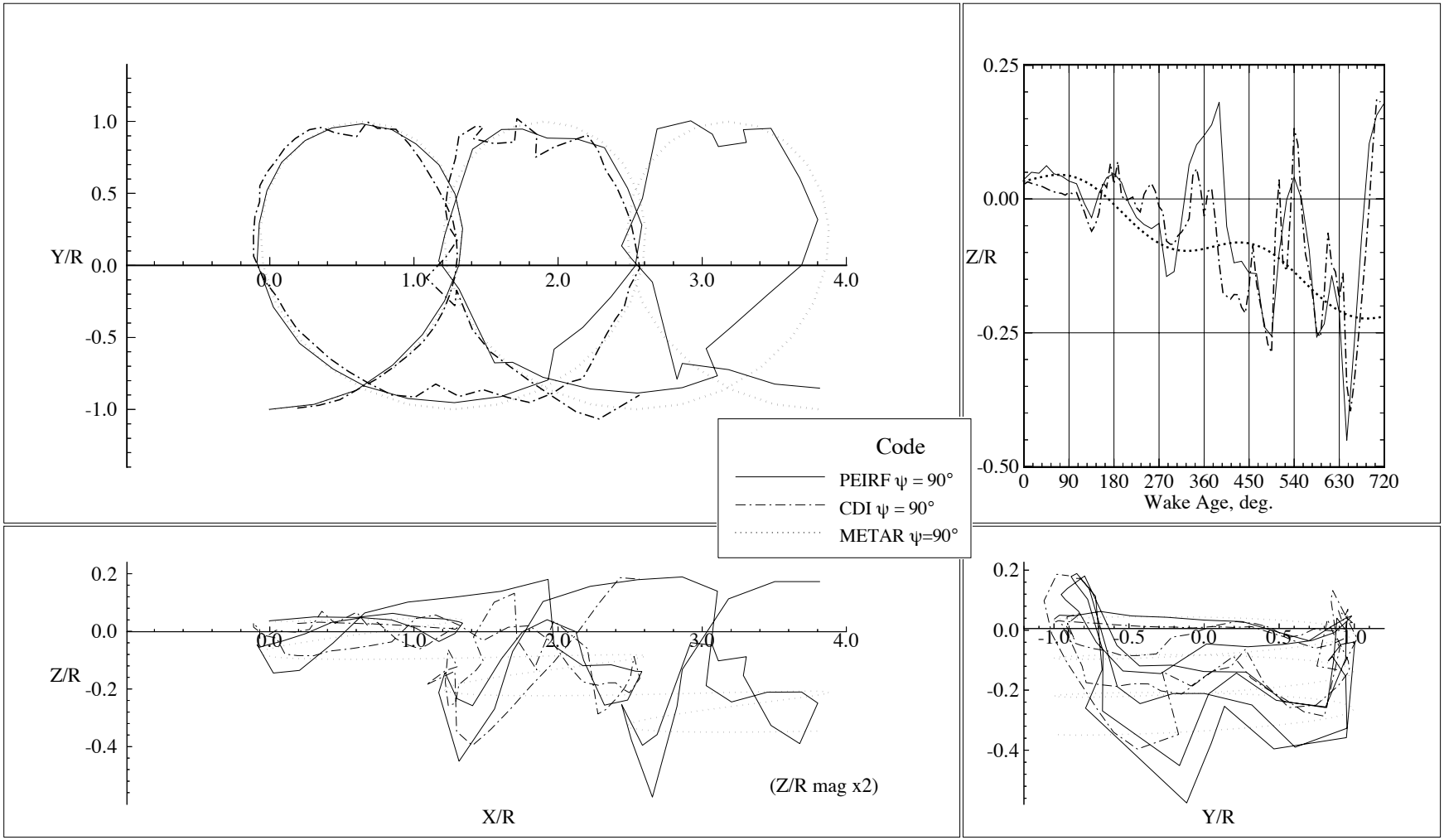

Figure 4-2: Wake geometry with rotor at ψ=90.0

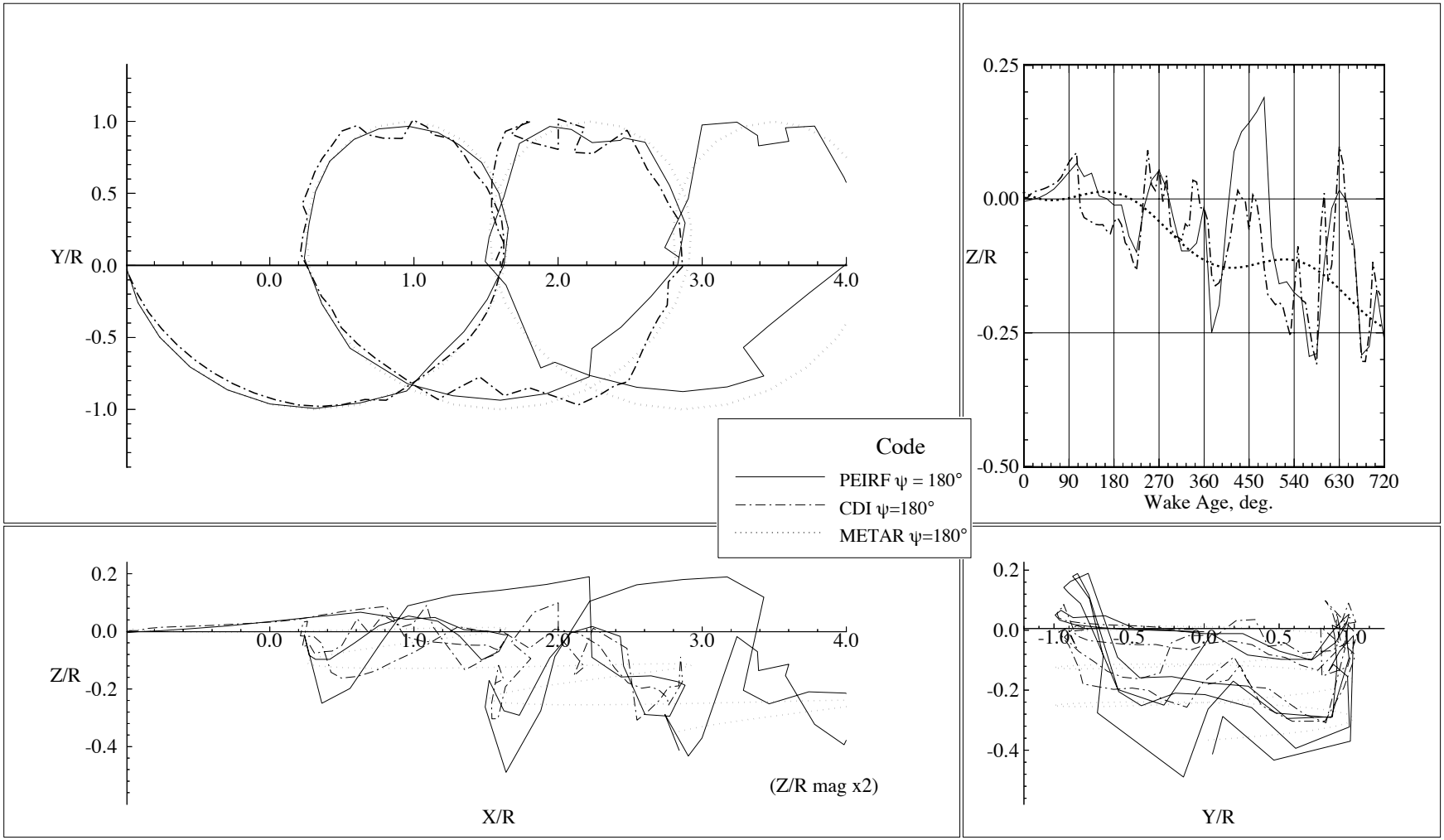

Figure 4-3: Wake geometry with rotor at ψ=180.0

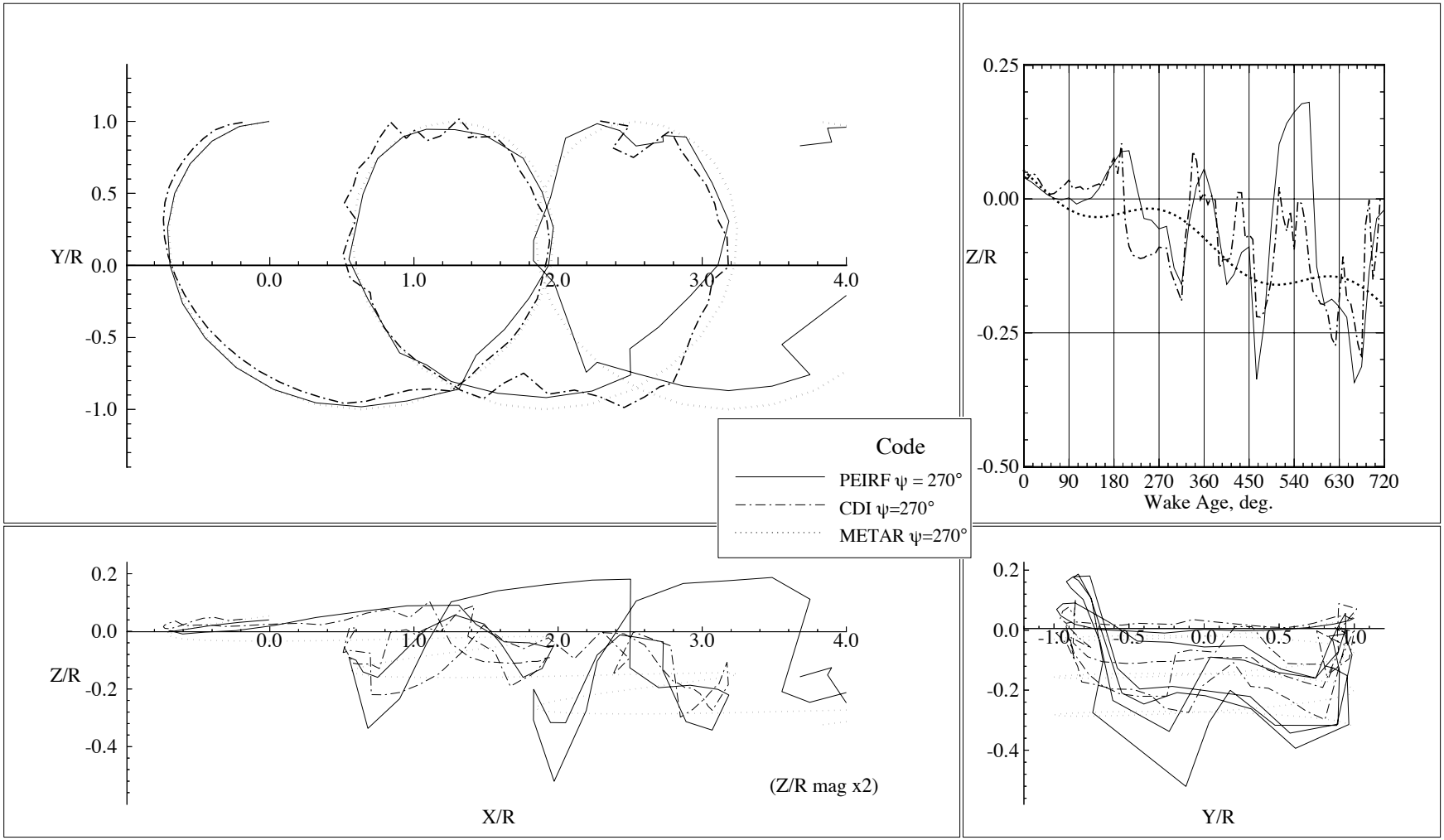

Figure 4-4: Wake geometry with rotor at ψ=270.0

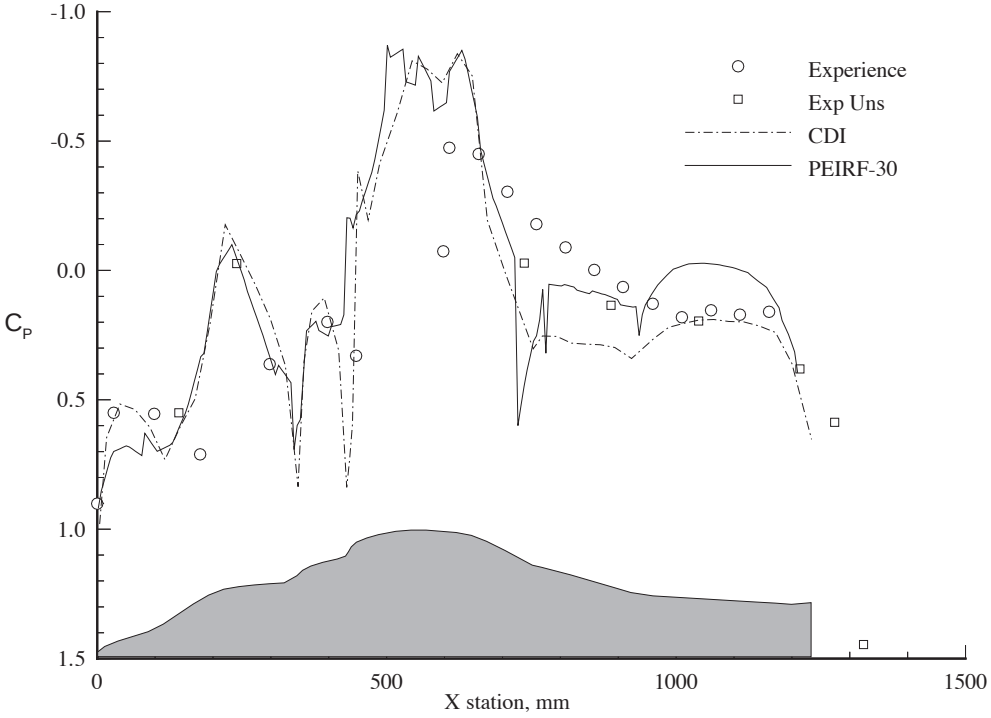

Figure 5-1: Mean pressure along dorsal line of fuselage

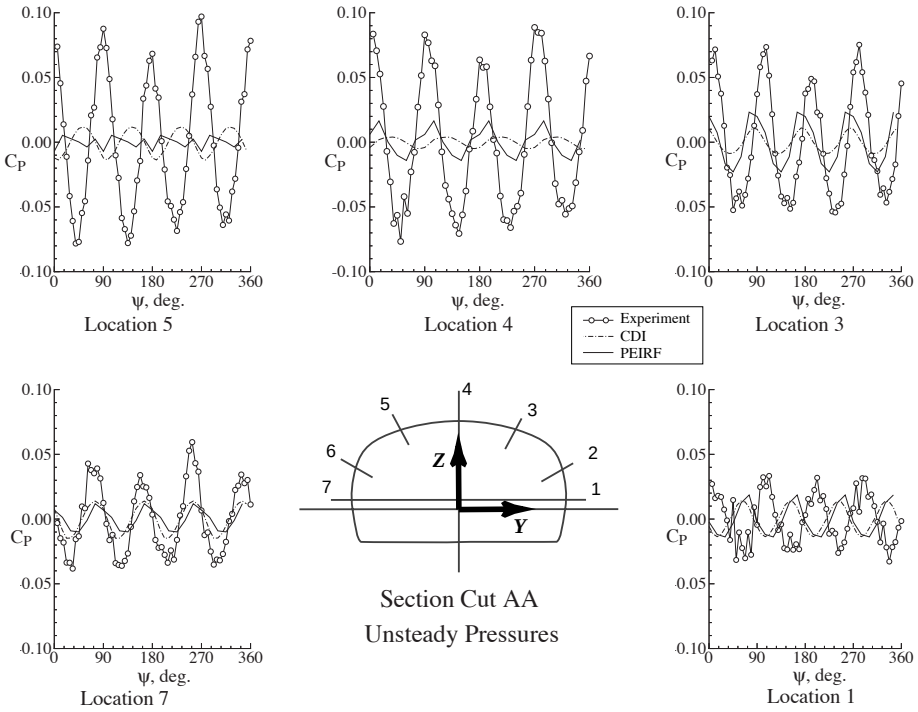

Figure 5-2: Unsteady pressures at fuselage station AA

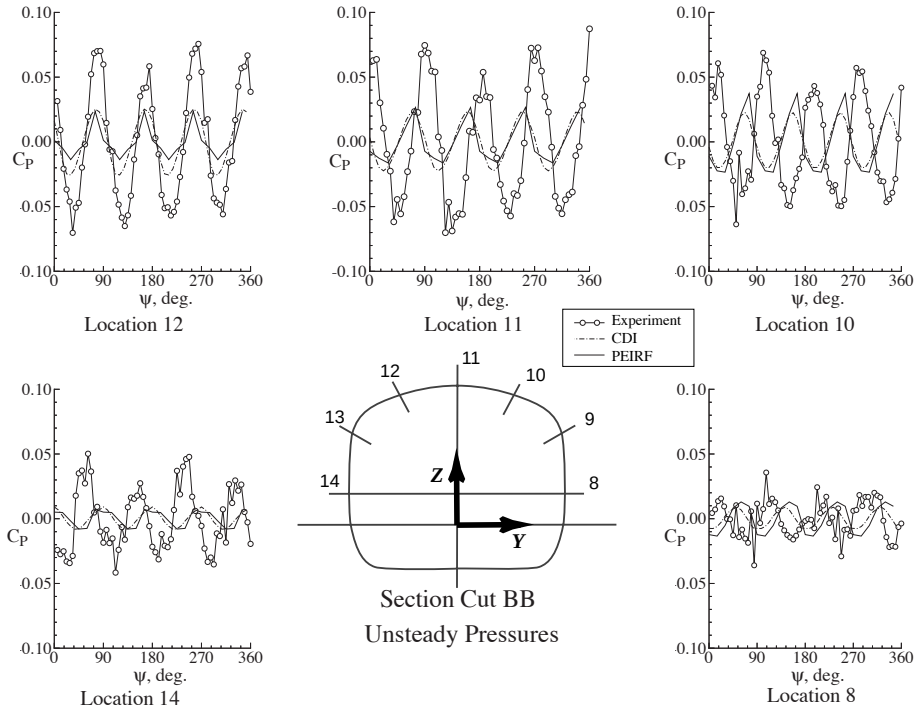

Figure 5-3: Unsteady pressures at fuselage station BB

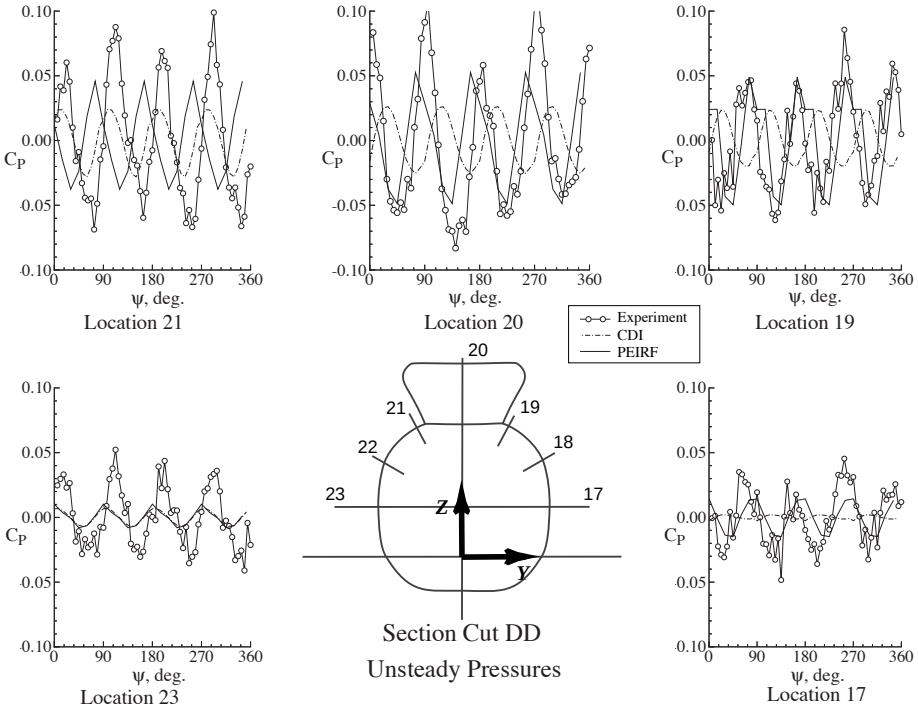

Figure 5-4: Unsteady pressures at fuselage station DD

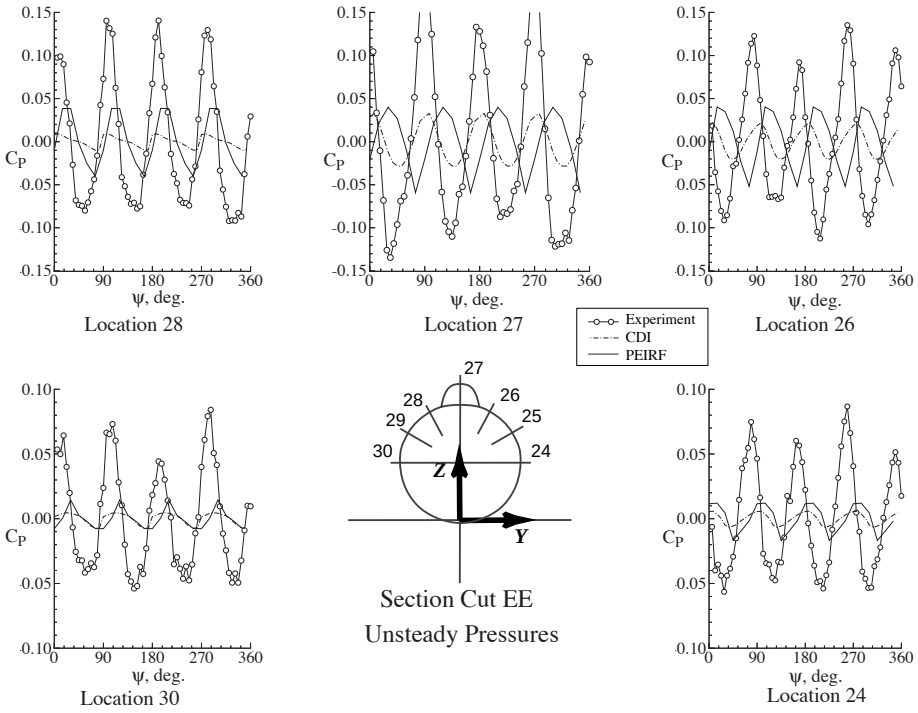

Figure 5-5: Unsteady pressures at fuselage station EE

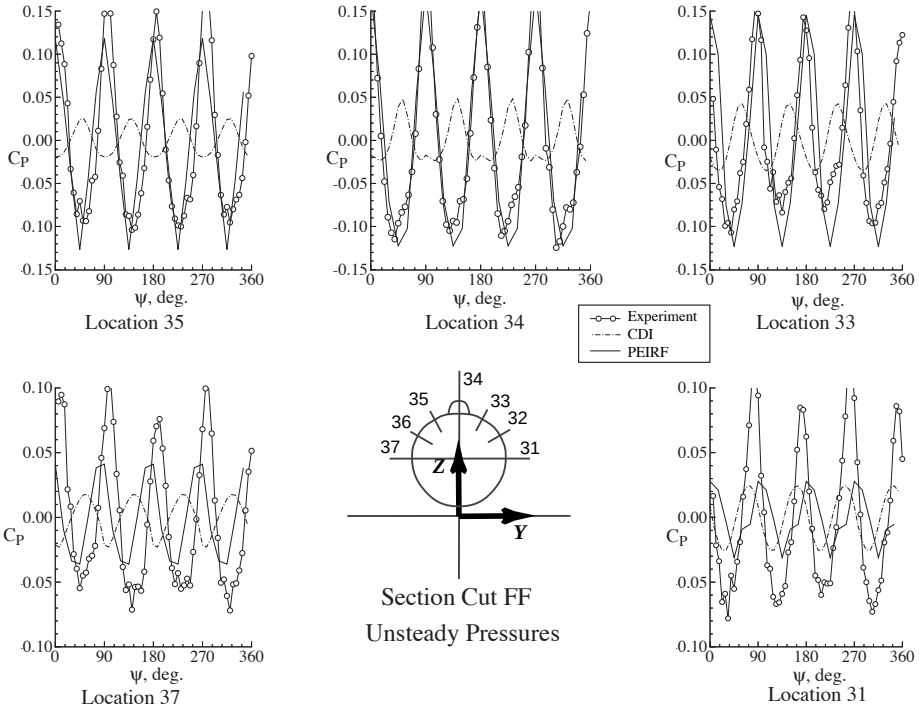

Figure 5-6: Unsteady pressures at fuselage station FF